Self-Similar Subgrid-Scale Models for Inertial Range Turbulence and Accurate Measurements of Intermittency

Luca Biferale,[1] Fabio Bonaccorso,[1] Michele Buzzicotti,[1] and Kartik P. Iyer[2]
[1]Department of Physics and INFN, University of Rome Tor Vergata, Via della Ricerca Scientifica 1, 00133, Rome, Italy
[2]Department of Mechanical and Aerospace Engineering, New York University, New York, New York 11201, USA

(Received 20 January 2019; revised manuscript received 31 March 2019; published 1 July 2019)

A class of spectral subgrid models based on a self-similar and reversible closure is studied with the aim to minimize the impact of subgrid scales on the inertial range of fully developed turbulence. In this manner, we improve the scale extension where anomalous exponents are measured by roughly 1 order of magnitude when compared to direct numerical simulations or to other popular subgrid closures at the same resolution. We find a first indication that intermittency for high-order moments is not captured by many of the popular phenomenological models developed so far.

DOI: 10.1103/PhysRevLett.123.014503

Turbulence is ubiquitous in nature and in engineering applications, and it is characterized by the presence of intense non-Gaussian fluctuations on a wide range of inertial scales and frequencies. The main mechanism to be controlled and eventually modeled is the energy transfer from the large-scale L where the flow is stirred to the small-scale η where viscous effects are dominant [1–5]. The Reynolds number is a measure of the separation between the two scales, $\mathrm{Re} \sim (L/\eta)^{4/3}$. For most applications, Re is too large to allow the problem to be attacked by direct numerical simulations (DNS) [4,6]. Similarly, fundamental problems connected to the presence of anomalous scaling [1,7–9] in the limit $\mathrm{Re} \to \infty$ cannot be easily studied using numerical tools. In such a deadlock, the applied community resorts to large eddy simulations (LES), a numerical approach that restricts the Navier-Stokes equations to a range of scales (or wave numbers) larger (smaller) than a given cutoff $r > r_c$ ($k < k_c$) and modeling all subgrid-scale (SGS) degrees of freedom with closures in configuration [3,10–12] or Fourier [13–16] space. The aim is to achieve good accuracy for the energy-containing modes without paying too much attention to those (inertial) scales that are fully resolved but also unavoidably affected by the subgrid-scale closure. As a matter of fact, most LES implementations successfully reproduce large-scale dynamics $k \ll k_c$ and are inaccurate for the highest resolved wave number modes $k \sim k_c$. This fact prevents the possibility for us to use LES models to improve our understanding of multiscale velocity fluctuations and/or the feedback of small-scale fluctuations on global mean profiles. In particular, SGS models (SGSM) perform very poorly concerning the properties of the inertial-range scaling of velocity structure functions (SF),

$$S_n(r) = \langle [\delta_r u]^n \rangle \sim \left(\frac{r}{L}\right)^{\zeta_n}, \tag{1}$$

where we defined the longitudinal increments $\delta_r u = [\boldsymbol{u}(\boldsymbol{r}+\boldsymbol{x}) - \boldsymbol{u}(\boldsymbol{x})] \cdot \hat{\boldsymbol{r}}$, and we have assumed isotropy and homogeneity. The exponents ζ_n in Eq. (1) are the key quantities to predict the asymptotic statistics for large Reynolds numbers, where r/L can be arbitrarily small. On one side, experiments and numerical simulations have provided much evidence that the scaling of $S_n(r)$ is anomalous, i.e., different from the Kolmogorov 1941 (K41) prediction $\zeta_n = n/3$ [7–9,17,18]. On the other hand, we do not have any first-principles derivations of ζ_n. Furthermore, it is extremely difficult to get accurate measurements of the exponents due to the concurrent requirements of having a large scaling range and large statistical ensembles. As a result, we also lack the numerical and experimental accuracy to distinguish among different phenomenological models [19–26]. Finally, few assessments exist of the robustness of the exponents with respect to the small-scale dissipative mechanism [27–30].

In this Letter, we introduce a class of subgrid models to minimize the impact of the SGS closure on the inertial range: A sort of perfect energy-cascade sink that achieves a much higher effective numerical resolution to study scaling properties in turbulence. The idea was already presented in Refs. [31,32] but was never applied and developed in the way it is here. We introduce a self-similar buffer close to the highest resolved mode, such as to have an ultraviolet boundary condition for the energy cascade at high k which is consistent with the existence of an infinitely extended inertial range. The advantages with respect to other closures are many. First, our model is time reversible, allowing the formation of backscatter events, too. Second, it is a minor modification of the high-wave-number dynamics, without touching the Fourier phases and therefore with a minimal impact on the formation of intense coherent events that are believed to be responsible for anomalous scaling. Unlike in Ref. [32], here we focus on high-Reynolds-number

applications to assess the impact of the closure on the inertial range properties. Furthermore, we expand the protocol by considering also a new Fourier modulation where the closure is applied such as to improve its efficiency in adsorbing the energy cascade.

In the following, we show that our LES protocol is able to obtain the same inertial range extension of a fully resolved viscous DNS while saving roughly 1 order of magnitude of resolution. As a result, considering also the gain due to the possibility of relaxing the time step, the improvement in the computational resources is larger than a factor of 1000, opening the way towards increased accuracy of measuring scaling exponents in turbulence, in both the scaling range extension and the statistical error. Moreover, we assess the universality issue with respect to the ultraviolet dissipation mechanism by comparing the scaling obtained with our SGS model with the ones measured in DNS and experiments [8,9,17]. Another by-product is to have a LES model that is accurate for small-scale evolution, something important for engineering applications that control extreme non-Gaussian events close to the subgrid cutoff [33–36].

The model.—Let us consider the Fourier-space evolution of the three-dimensional Navier-Stokes equations in a periodic box of size $L = 2\pi$ and resolved with N grid points per direction and maximum wave number in all directions given by $k_{\max} = N/2$:

$$(\partial_t + \nu k^2)\hat{\boldsymbol{u}}_{\boldsymbol{k}}(t) = \hat{\boldsymbol{T}}_{\boldsymbol{k}}(t) + \hat{\boldsymbol{f}}_{\boldsymbol{k}}(t), \tag{2}$$

where ν is the viscosity, $\hat{\boldsymbol{f}}_{\boldsymbol{k}}(t)$ is the Fourier transform of the external forcing, and $\hat{\boldsymbol{T}}_{\boldsymbol{k}}(t) = -i\boldsymbol{k}\cdot[\mathbb{I} - (\boldsymbol{k}\otimes\boldsymbol{k}/|k|^2)]\times[\sum_{\boldsymbol{k}'}\hat{\boldsymbol{u}}_{\boldsymbol{k}'}(t)\otimes\hat{\boldsymbol{u}}_{\boldsymbol{k}'-\boldsymbol{k}}(t)]$ is the nonlinear term. We follow Ref. [32] and we replace the viscous term on the lhs of Eq. (2) with a nonlinear inertial closure that imposes a perfect self-similar Kolmogorov-like spectrum in a k window close to the ultraviolet cutoff $k_{\max}$:

$$E_k(t) = (k/k_c)^{-(5/3)}E_{k_c}(t); \quad k_c \le k \le k_{\max}, \tag{3}$$

where $E_k(t) = \frac{1}{2}\sum_{|\boldsymbol{k}|=k}|\hat{\boldsymbol{u}}_{\boldsymbol{k}}(t)|^2$. The LES equation for the resolved velocity field equipped with the fixed-spectrum SGS model can be written using a Lagrangian multiplier $\lambda_k(t)$ [31],

$$\partial_t\hat{\boldsymbol{u}}_{\boldsymbol{k}}(t) = \hat{\boldsymbol{T}}_{\boldsymbol{k}}(t) + \hat{\boldsymbol{f}}_{\boldsymbol{k}}(t) - \gamma_{\boldsymbol{k}}\lambda_k(t)\hat{\boldsymbol{u}}_{\boldsymbol{k}}(t), \tag{4}$$

where we have removed the viscosity, and $\gamma_{\boldsymbol{k}}$ is a projector which selects the range of scales where the subgrid closure acts: $\gamma_{\boldsymbol{k}} = 0$ if $k \le k_c$ and $\gamma_{\boldsymbol{k}} = 1$ if $k_c < k < k_{\max}$ (sharp SGSM). It is easy to realize that in order to satisfy Eq. (3), we can impose $dE_k/dt = (k_c/k)^{5/3}dE_{k_c}/dt$ and choose $\lambda_k(t)$ to be

$$\lambda_k(t) = \frac{1}{2}\frac{T_k(t) - (k/k_c)^{-5/3}T_{k_c}(t)}{E_k(t)}, \tag{5}$$

where $T_k(t)$ is the transfer function: $T_k(t) = \sum_{|\boldsymbol{k}|=k}\hat{\boldsymbol{u}}^*_{\boldsymbol{k}}(t)\hat{\boldsymbol{T}}_{\boldsymbol{k}}(t)$. In order to mitigate the sharp transition across the SGS k_c, we also explored another protocol where the percentage of constrained modes grows linearly from 0 at k_c to 1 at $k_{\max}$. To do that, we define a (quenched) probability to apply the SGS model at any given wave number as follows (smooth SGSM):

$$\gamma_{\boldsymbol{k}} = \begin{cases} 0 & \text{if } k < k_c, \\ 1 & \text{with prob } P_k = \frac{k-k_c}{k_{\max}-k_c} \text{ if } k_c \le k < k_{\max}. \end{cases} \tag{6}$$

In this way, only a fraction of modes $(k-k_c)/(k_{\max}-k_c)$ will be affected by the constraint for any given shell k, such that we move from fully unconstrained dynamics (for $k < k_c$) to fixed-spectrum dynamics (for $k = k_c$) with continuity (see inset of Fig. 1 for a graphical scheme of the Fourier-space support of the projector $\gamma_{\boldsymbol{k}}$ for both sharp and smooth SGSM cases). We also anticipate that in order to minimize the transition across k_c, we will need to keep a small residual viscosity ν even when using the self-similar closure. This is unavoidable due to the fact that the closure acts on a finite range of scales and cannot exactly mimic the SGS dynamics at infinite Reynolds number.

Results.—We compare the LES data obtained at a resolution of 1024^3 with the two different DNS resolutions: one identical to the LES (DNS × 1) and one taken from a state-of-the-art study at 8192^3 collocation points [8] denoted (DNS × 8). All runs are forced with a white-in-time Gaussian forcing acting at $k_f \in [1, 1.5]$ for DNS × 1 and a $k_f \in [1, 3]$ for DNS × 8. More details on the numerical setup can be found in Table I. In Fig. 1, we

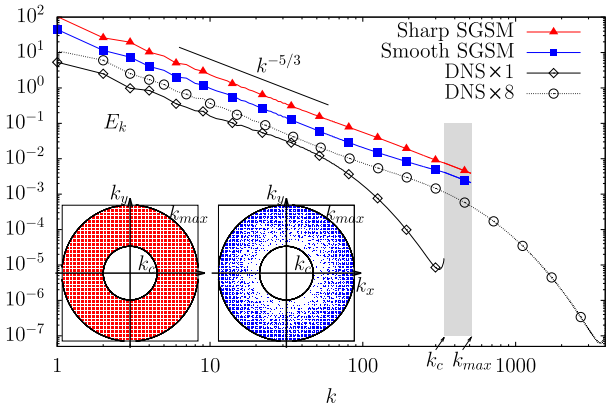

FIG. 1. Energy spectra for the simulations in Table I. The curves are shifted vertically for the sake of presentation. The gray area marks the range of wave numbers where the closure acts. Inset: 2D sketch of the Fourier-space support where $\gamma_{\boldsymbol{k}} = 1$. Left and right panels represent, respectively, the sharp SGSM and smooth SGSM cases.

TABLE I. Simulations: N is the number of collocation points in each spatial direction, k_c the smallest wave number where the SGS closure acts, $k_{\max}$ the maximum wave number evolved by the dynamics, ϵ the mean energy injection, and ν the kinematic viscosity. $\mathrm{Re} = \epsilon^{1/3}L^{4/3}/\nu$ is the Reynolds number with $L = 2\pi$. T is the duration of simulations in units of the eddy turnover time $\epsilon^{-1/3}L^{2/3}$.

	N	k_c	$k_{\max}$	ϵ	ν	T	Re
Sharp SGSM	1024	340	512	3.0	8.0×10^{-5}	8.5	2.1×10^5
Smooth SGSM	1024	340	512	3.0	4.0×10^{-5}	8.5	4.2×10^5
DNS × 1	1024	⋯	340	2.5	8.0×10^{-4}	12	2.0×10^4
DNS × 8	8192	⋯	3861	1.5	4.4×10^{-5}	3.4	3.0×10^5

show the spectral properties of all data. Our closure reproduces the same extension of the scaling range of DNS × 8 and considerably extends the one obtained with DNS × 1. We obtain an inertial behavior for all k in the LES model without the viscous range of scales needed with standard viscosity in DNS × 8.

Anomalous scaling of high-order SF.—To assess the scaling properties in a quantitative way, we measure the local scaling exponents

$$\xi_n(r) = \frac{d\log S_n(r)}{d\log(r)}, \tag{7}$$

where in the presence of pure power laws, we must have $\xi_n(r) = \mathrm{const} = \zeta_n$.

By measuring where $\xi_n(r)$ is constant, we have an unbiased definition of the inertial range extension, and we can assess scale by scale the quality of our data. In particular, the intermittency and scale-dependent corrections from Gaussian behavior can be measured by the deviation from zero of $\Delta_n(r) = \xi_n(r)/\xi_2(r) - n/2$, as seen by expressing the generalized flatness in terms of the second-order SF:

$$F_n(r) = \frac{S_n(r)}{[S_2(r)]^{n/2}} \sim [S_2(r)]^{\{[\xi_n(r)/\xi_2(r)]-(n/2)\}}.$$

In Fig. 2, we show $\xi_2(r)$ for our two SGSM closures and compare them with the same quantity measured on DNS × 1 and DNS × 8. As shown for the spectral case, LES data have a much larger extension of scaling than DNS × 1, matching the DNS obtained with an 8-times-larger resolution (DNS × 8).

Despite the existence of a *plateau* for $\xi_2(r)$ for all data, the constraint $\xi_2(r) \to 2$ for $r \to 0$ makes the jump from inertial to viscous values too big, and it is very difficult to quantitatively distinguish the K41 scaling from any intermittent phenomenological model as, e.g., the SL model [22], the Yakhot model [26], and the model proposed by Oz

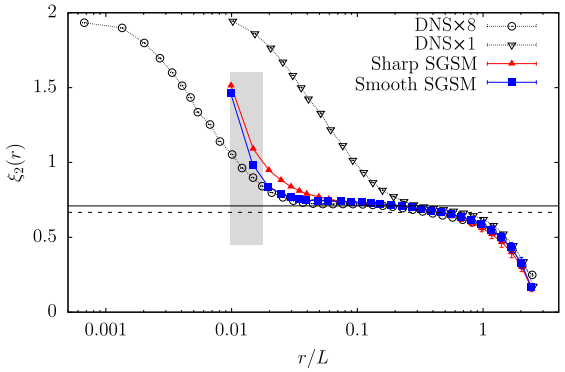

FIG. 2. Log-lin plot of $\xi_2(r)$ vs r. Solid and dashed lines indicate the SL $\zeta_2 = 0.69$ and K41 $\zeta_2 = 2/3$ predictions, respectively. In gray, we indicate the range of scales where the closure (5) is acting. Error bars are comparable with symbol sizes.

based on spontaneous symmetry breaking of dilation invariance and random geometry [24,37,38]. To be more accurate, in Fig. 3 we show the scaling of the generalized flatness (inset) and of the scale-by-scale ratio $\Delta_n(r) + n/2 = \xi_n(r)/\xi_2(r)$ (main panel) for $n = 4, 6$. Here, a Kolmogorov-like nonanomalous scaling corresponds to a constant value $n/2$ for all r. As one can see, the deviation from the Kolmogorov scaling is now evident, and much more importantly, our SGSM closures are able to develop an inertial range as extended as the DNS × 8 case, if not even larger. Moreover, the smooth SGSM closure is a bit better than the sharp SGSM case. We consider these results a clear demonstration that the SGS model developed here can be considered a sort of infinite-Reynolds-number closure. Considering the fact that by using the smooth SGSM closure we can achieve the same accuracy for local exponents of a DNS with 8-times-larger resolution, we estimate a gaining factor 8^3 for the spatial grid, which together with the less stringent Courant-Friedrichs-Lewy condition for the time integration $\sim\epsilon^{-1/3}k_{\max}^{-2/3}$ leads to a total gain close to a factor of 1000. In Table II, we present a summary of the scaling properties of $F_n(r)$ from where it is clear that the SGS models agree with the DNS × 8 and with the prediction made by the SL, Yakhot, and EO models for moment $n = 6, 8$, while for the largest achievable order $n = 10$, the numerical data are more intermittent than all three phenomenological models (see also the Supplemental Material [39]).

A few comments are now in order. First, it is useful to preserve a very small viscous term in Eq. (4) in order to have a smooth transition across k_c. This is implemented in our approach, keeping a term $\nu k^2 \hat{\boldsymbol{u}}_{\boldsymbol{k}}(t)$ with a very small ν as shown in Table I. It is clear from Fig. 3 that even by optimizing ν, there exists in the SGSM a *pseudoviscous* range (extended over a few grid points) where scaling breaks down. This is unavoidable because our closure is acting in the Fourier space and does not enforce any pure

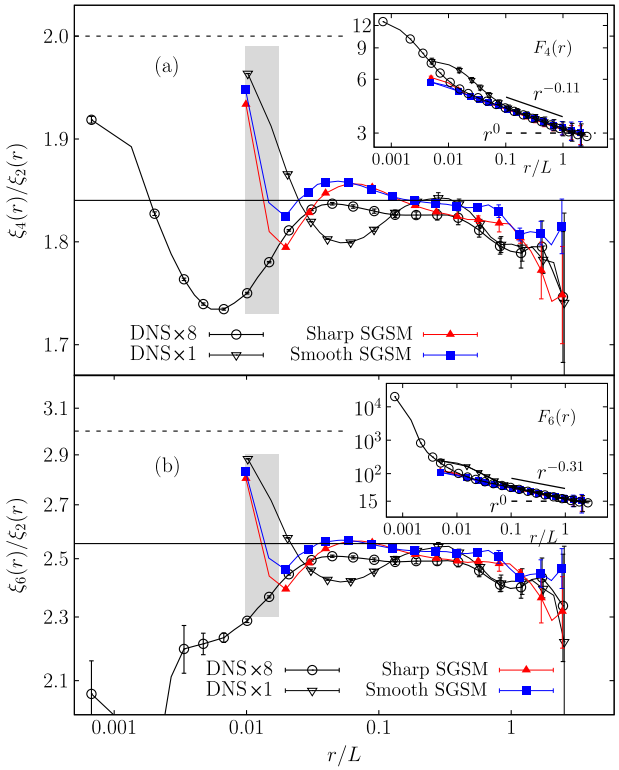

FIG. 3. Log-lin plot of $\xi_n(r)/\xi_2(r)$ for (a) $n = 4$ and (b) $n = 6$ for SGSM and DNS data. K41 and SL predictions are given by the dashed and solid lines, respectively. EO and Yakhot models are very close to SL predictions for these two moments (see Table II). In gray we indicate the range of scales where the closure (5) is applied. Inset: log-log plot of $F_n(r)$ vs r (same symbols as the main panel). SL and K41 scaling are given by the solid and the dashed lines, respectively. In all figures, errors are evaluated from the scatter of 40 configurations.

scaling for the high-order SFs. The existence of a small bump for the local slopes around the transition from the viscous to inertial range is also present in experimental data at high Reynolds number [9]. On the other hand, the efficiency in extending the anomalous scaling range is good evidence that to capture intermittency the SGSM must maintain the correct phase correlations [40], which is one of the main added values of Eq. (5). Second, the smooth projector recipe is not unique, and one can imagine many different ways to enforce the transition from modes that evolve according to their Euler dynamics ($k < k_c$) to those that feel the spectral constraint. In particular, once the controlled buffer is introduced and it is large enough, one might imagine even avoiding the dealiasing protocol and keeping $k_{\max} = N/2$ as done here. The effects of introducing dealiasing are minor and discussed in Fig. 2 of the Supplemental Material [39]. We now discuss the comparison with two other popular ways to *enhance* the effective Reynolds numbers. In Fig. 4, we compare the flatness obtained from a DNS with hyperviscosity [29,41] or from a Smagorinsky SGS model [10,11,36] with the one proposed here. Notice that the hyperviscous data are only qualitatively as good as the smooth SGSM, as shown by the fact that the former has a less extended plateau with respect to the latter. There is no doubt that the closure (5) is superior to both the Smagorinsky and hyperviscous models. Finally, we mention that from Eq. (4), one can define a Galilean-invariant [42] SGS energy transfer: $\Pi(\boldsymbol{x}) = \partial_i u_j(\boldsymbol{x}) \int d\boldsymbol{k} \gamma_{\boldsymbol{k}} \lambda_k e^{i\boldsymbol{k}\cdot\boldsymbol{x}} i k_i / k^2 \hat{u}_{j,\boldsymbol{k}}$, which is nonpositive definite and therefore able to reproduce backscatter events.

Conclusions.—We have shown that a self-similar SGS model is able to extend the anomalous scaling to almost the entire range of resolved scales. This protocol reduces the computational cost by a factor of 1000 compared to a fully resolved DNS, with the same inertial range extension. The agreement between the scaling observed with the SGSM and that measured by DNS and experiments supports the universality of the inertial range dynamics with respect to the energy-absorbing mechanism at small scales. Thanks to the unprecedented accuracy in the determination of the scaling properties, we have been able to find a small discrepancy between the numerical data and the predictions by some of the most popular phenomenological models [22,24,26] for high order moments. It remains an open key question to check if our closure remains accurate also at higher resolution. If this is indeed the case, we have a chance to make a discontinuous improvement in the assessment of scaling properties in homogeneous and isotropic turbulence.

TABLE II. $\bar{\Delta}_n + n/2$ obtained as a fit of $\xi_n(r)/\xi_2(r)$ for $r \in [0.03:0.9]L$ for smooth SGSM and DNS × 8, and for $r \in [0.15:0.9]L$ for DNS × 1. Errors for the numerical data refer to the sum among statistical fluctuations and the variations considered by fitting in the first or second half of the scaling range (see the Supplemental Material [39] for more details). The last three columns give the prediction from the She-Leveque (SL) [22], Yakhot [26], and Eling-Oz (EO) [24] models, where the last two have been fitted to have the value for $n = 4$ identical to the smooth SGSM case. Errors in the Yakhot and EO models are estimated by fixing their free parameter to match either the maximum SGSM value 1.843 + 0.015 or the minimum 1.843–0.015 for $n = 4$; see the Supplemental Material [39].

	SGSM	DNS × 1	DNS × 8	SL	Yakhot	EO
$n = 4$	1.843(15)	1.828(25)	1.824(18)	1.839	1.843(15)	1.843(15)
$n = 6$	2.537(38)	2.501(78)	2.485(39)	2.555	2.563(38)	2.586(35)
$n = 8$	3.092(30)	3.034(147)	2.982(56)	3.176	3.186(66)	3.257(58)
$n = 10$	3.504(81)	3.440(230)	⋯	3.727	3.730(96)	3.875(83)

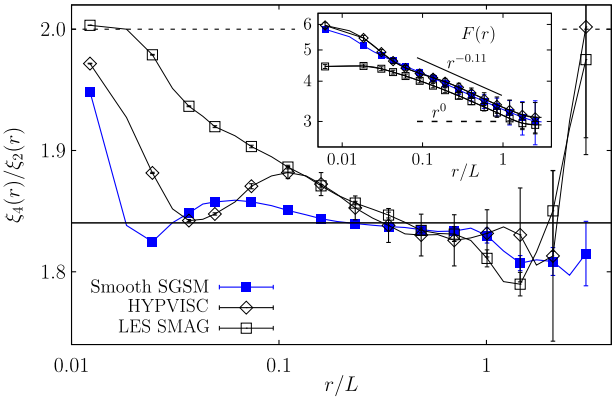

FIG. 4. Comparison of $\xi_4(r)/\xi_2(r)$ for smooth SGSM, Smagorinsky LES, and hyperviscous DNS with $\nu\Delta^2\boldsymbol{u}$ and $\nu = 2.0 \times 10^{-8}$. All simulations have 1024^3 collocation points. The SL and K41 predictions are given by the solid and the dashed lines, respectively. Inset: $F_4(r)$ for the same data.

Our model outperforms other common closures such as the Smagorinsky model or hyperviscous DNS. Fully time-reversible models might be of theoretical interest for the application of the chaotic hypothesis [43]. In addition to the self-similar properties, another advantage of our SGS closure is that the phase dynamics is left untouched. Because of its generality, the closure can be applied to a broad set of other flow configurations such as rotating, stratified, or magnetohydrodynamic turbulence, including stiff problems as the kinematic dynamo in the limit of small Prandtl numbers [44]. Similarly, one might imagine applications to wall bounded flows where small-scale anisotropy is negligible [45] by imposing scaling laws on the spectral degrees of freedom in planes parallel to the wall (homogeneous directions), with properties dependent on the distance from the wall.

We acknowledge useful discussions with R. Benzi, M. Bustamante, M. Linkmann, C. Meneveau, Y. Oz, M. Sbragaglia, K. R. Sreenivasan, P. K. Yeung, and M. Wilczek and funding from the European Union Programme (FP7/2007-2013) Grant No. 339032. L. B. acknowledges the hospitality of the Center for Environmental and Applied Fluid Mechanics at Johns Hopkins University where this work was started. Part of the simulations have been done at BSC-CNS (PRACE Grant No. 188513).

[1] U. Frisch, *Turbulence: The Legacy of A. N. Kolmogorov* (Cambridge University Press, Cambridge, England, 1995).
[2] K. R. Sreenivasan, Rev. Mod. Phys. **71**, S383 (1999).
[3] S. B. Pope, *Turbulent Flows* (Cambridge University Press, Cambridge, England, 2000).
[4] T. Ishihara, T. Gotoh, and Y. Kaneda, Annu. Rev. Fluid Mech. **41**, 165 (2009).
[5] A. Alexakis and L. Biferale, Phys. Rep. **767–769**, 1 (2018).
[6] J. Jiménez, Annu. Rev. Fluid Mech. **44**, 27 (2012).
[7] R. Benzi, L. Biferale, R. Fisher, D. Lamb, and F. Toschi, J. Fluid Mech. **653**, 221 (2010).
[8] K. P. Iyer, K. R. Sreenivasan, and P. K. Yeung, Phys. Rev. E **95**, 021101(R) (2017).
[9] M. Sinhuber, G. P. Bewley, and E. Bodenschatz, Phys. Rev. Lett. **119**, 134502 (2017).
[10] J. Smagorinsky, Mon. Weather Rev. **91**, 99 (1963).
[11] C. Meneveau and J. Katz, Annu. Rev. Fluid Mech. **32**, 1 (2000).
[12] M. Lesieur, O. Métais, and P. Comte, *Large-Eddy Simulations of Turbulence* (Cambridge University Press, Cambridge, England, 2005).
[13] R. H. Kraichnan, J. Atmos. Sci. **33**, 1521 (1976).
[14] J.-P. Chollet and M. Lesieur, J. Atmos. Sci. **38**, 2747 (1981).
[15] J. Baerenzung, H. Politano, Y. Ponty, and A. Pouquet, Phys. Rev. E **77**, 046303 (2008).
[16] L. Biferale, A. A. Mailybaev, and G. Parisi, Phys. Rev. E **95**, 043108 (2017).
[17] T. Gotoh, D. Fukayama, and T. Nakano, Phys. Fluids **14**, 1065 (2002).
[18] T. Watanabe and T. Gotoh, J. Fluid Mech. **590**, 117 (2007).
[19] A. N. Kolmogorov, J. Fluid Mech. **13**, 82 (1962).
[20] R. Benzi, G. Paladin, G. Parisi, and A. Vulpiani, J. Phys. A **17**, 3521 (1984).
[21] C. Meneveau and K. R. Sreenivasan, Phys. Rev. Lett. **59**, 1424 (1987).
[22] Z.-S. She and E. Leveque, Phys. Rev. Lett. **72**, 336 (1994).
[23] J. Schumacher, K. R. Sreenivasan, and V. Yakhot, New J. Phys. **9**, 89 (2007).
[24] C. Eling and Y. Oz, J. High Energy Phys. 15 (2015) 150.
[25] V. Yakhot and D. Donzis, Phys. Rev. Lett. **119**, 044501 (2017).
[26] V. Yakhot, Phys. Rev. E **63**, 026307 (2001).
[27] G. Falkovich, Phys. Fluids **6**, 1411 (1994).
[28] D. Lohse and A. Müller-Groeling, Phys. Rev. Lett. **74**, 1747 (1995).
[29] U. Frisch, S. Kurien, R. Pandit, W. Pauls, S. S. Ray, A. Wirth, and J.-Z. Zhu, Phys. Rev. Lett. **101**, 144501 (2008).
[30] D. A. Donzis and K. Sreenivasan, J. Fluid Mech. **657**, 171 (2010).
[31] Z.-S. She and E. Jackson, Phys. Rev. Lett. **70**, 1255 (1993).
[32] J. Jimenez, Center for Turbulence Research. Annual Research Briefs (Standford University, 1993), p. 171.
[33] R. J. Stevens, M. Wilczek, and C. Meneveau, J. Fluid Mech. **757**, 888 (2014).
[34] R. J. Stevens and C. Meneveau, Annu. Rev. Fluid Mech. **49**, 311 (2017).
[35] M. Buzzicotti, M. Linkmann, H. Aluie, L. Biferale, J. Brasseur, and C. Meneveau, J. Turbul. **19**, 167 (2018).
[36] M. Linkmann, M. Buzzicotti, and L. Biferale, J. Turbul. **19**, 493 (2018).
[37] Y. Oz, arXiv:1809.10003.
[38] Y. Oz, Eur. Phys. J. C **78**, 655 (2018).
[39] See Supplemental Material at http://link.aps.org/supplemental/10.1103/PhysRevLett.123.014503for auxiliary information on error estimates in the structure function calculations..
[40] B. P. Murray and M. D. Bustamante, J. Fluid Mech. **850**, 624 (2018).

[41] V. Borue and S. A. Orszag, Phys. Rev. E **51**, R856 (1995).
[42] G. L. Eyink and H. Aluie, Phys. Fluids **21**, 115107 (2009).
[43] G. Gallavotti, Phys. Rev. Lett. **77**, 4334 (1996).
[44] S. Tobias, F. Cattaneo, and S. Boldyrev, in *MHD Dynamos and Turbulence, Ten Chapters in Turbulence*, edited by P. Davidson, Y. Kaneda, and K. R. Sreenivasan (Cambridge University Press, Cambridge, England, 2013).
[45] L. Biferale and I. Procaccia, Phys. Rep. **414**, 43 (2005).